Thermal absorption properties of ultra-thin metal layers on diamond surfaces

Alexander Harker

This thesis is submitted in partial fulfilment of the requirements for the Honours degree of BSc at the University of Bristol

26th April 2013

Abstract

Samples of microcrystalline diamond were etched with nickel using a hydrogen plasma treatment. Different temperatures and pressures were used during the treatment to create different surface morphologies. The three dimensional surface structuring and plasmonic effects acting upon the optical absorption of the diamond were studied. It was found that surface texturing had a larger impact upon absorption than plasmonic effects.

Acknowledgements

Contents

Introduction

Photovoltaic devices convert sunlight into electricity, mass use of them allowing the generation of electrical power on a large scale. It is a rapidly expanding global market, growing from a worldwide installed capacity of 69 GW[1] in 2011 to over 100 GW in February 2013[2]. Figure 1[1] illustrates the rapid growth of the industry in the past decade.
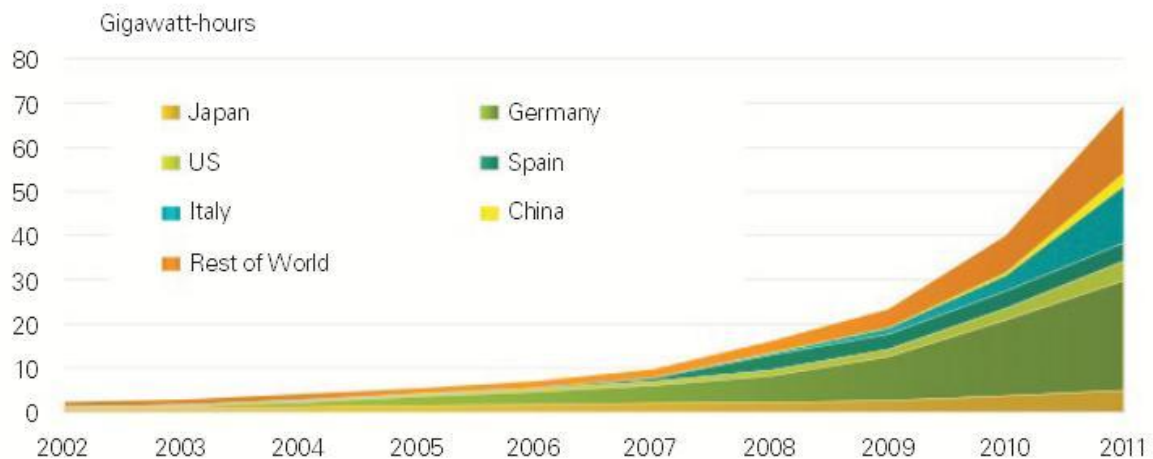

Solar PV generation capacity

Figure 1

The availability of sunlight to the world is only limited in the extreme northern and southern latitudes, meaning photovoltaics can be used globally. They have the potential to become competitive with fossil fuels and to make a considerable contribution to solving the increasing demand for energy worldwide.

Photovoltaic cells work via the photovoltaic effect, where electric current is created when a material's surface is exposed to electromagnetic radiation. This is due to excitation of electrons from the valence band to the conduction band of a conductor, or semi-conductor, by absorption of a photon of an appropriate frequency. These bands form due to the splitting of molecular orbitals in a solid. Electrons in an isolated atom occupy discrete energy levels, known as atomic orbitals.
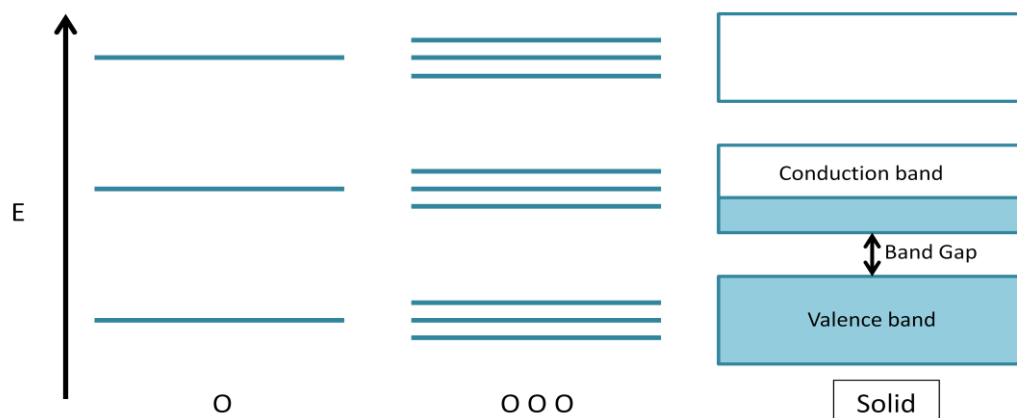

Figure 2

Figure 2 illustrates that when multiple atoms are brought together in a molecule or solid, the atomic orbitals split into molecular orbitals, each with their own energy. This is due to the Pauli exclusion principle, which states that no two electrons can occupy the same quantum state. When many

orbitals of similar energy are brought together they form bands. Figure 2 also shows a fully occupied valence band, and a partially occupied conduction band. Bands describe ranges of energies that electrons may have while in a solid, and the gaps between those bands are energy levels that electrons may not occupy. Valence bands are completely occupied by electrons and there are no free energy levels within the band to which electrons can move. Conduction bands are vacant or partially filled bands, where there is a high density of energetically available states that electrons can easily move to and from. This is where the Fermi level lies inside a band. The Fermi level is the energy below which electrons are expected to reside at thermodynamic equilibrium. Insulators have filled valence bands with large band gaps, so it is difficult for an electron to gain enough energy to be excited to a conduction band. In these material the Fermi level is within the band gap. Conductors have electrons in conduction bands where there are free to move and allow electric current to flow. Semi-conductors have no partially filled bands, only full valence bands. However, the band gap is small, usually 4 eV and below. This allows electrons to more easily be promoted to the conduction band. The current conduction in a semiconductor occurs via the free electrons and the 'holes' the electrons have left behind in the valence band. 'Doping' semiconductors, replacing atoms of the semiconductor with atoms which have a higher or lower number of valence electrons increases the number of charge carriers. Silicon, the major component of conventional solar cells, is a semiconductor.
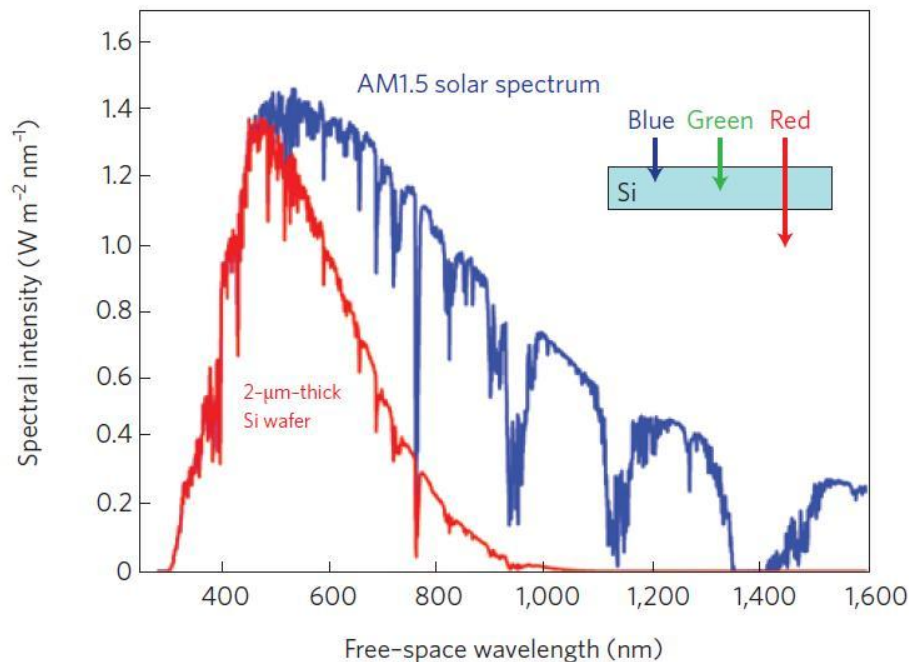

Figure 3

As solar radiation passes through the atmosphere it is attenuated by scattering and absorption, giving rise to the solar spectrum observed at sea level. Figure 3[3] shows the standard AM1.5 solar spectrum alongside a graph that illustrates the fraction of the solar spectrum absorbed by single pass through a 2 μm thick crystalline silicon film. It is shown that there is poor absorption by the silicon in the 600-1000 nm range. To oppose this, a majority of photovoltaic devices are manufactured using crystalline silicon wafers with thicknesses between 180-300 μm[3]. This increases the optical path length through the cell and therefore absorption of light and the subsequent generation of charge carriers. The expense in the production of these devices is due to the manufacture and processing of the amount of silicon material required, therefore there is a drive to find methods to decrease the amount of material used without sacrificing performance. To achieve this photovoltaic absorbers must be made to have as large an optical path length through them as

possible to ensure near complete absorption of incident radiation, and use the minimal amount of material necessary.

Thin film solar cells have film thicknesses of 1-2 μm[3,4], drastically reducing the amount of material utilised, and therefore cost per cell. They can be deposited on low cost substrates such as glass, plastic and stainless steel, and they are made from a variety of semi-conductors such as amorphous or polycrystalline silicon, gallium arsenide or cadmium telluride. They provide a low cost alternative to conventional silicon solar cells. However, reducing the thickness of the cell has one obvious drawback; a reduction in the optical path length through the cell, meaning lower efficiencies when compared to conventional cells.

Physically structuring the surface of solar cells to trap the light inside and maximise solar absorption is important to thin film solar cells to allow them to compete with conventional silicon solar cells. With this technique of 'light trapping', cells are designed so that the optical path length through them is much greater than their thickness[5]. In conventional silicon solar cells, increasing the effective path length of the cell is generally achieved using a pyramidal or rough surface structures to scatter light over a large angular range. With this texturing the absorption enhancement achieved can be described as $4n^2$, where n is the refractive index of the cell material[6,7]. This is much improved from non-textured cells. Texturing thin films is possible, albeit not on the same scale as conventional cells, so high efficiency can be maintained whilst thickness reduced, and constraints on silicon quality can be relaxed since the diffusion length of the minority charge carriers can be reduced proportionally to the intensity enhancement[6]. Conventional surface geometries are not suitable for thin film solar cells because the surface roughness would surpass the film thickness, and the increased surface area would increase minority charge carrier recombination in the surface and junction regions[3]. Texturing the substrate is possible, but again increased recombination losses are a result[8].
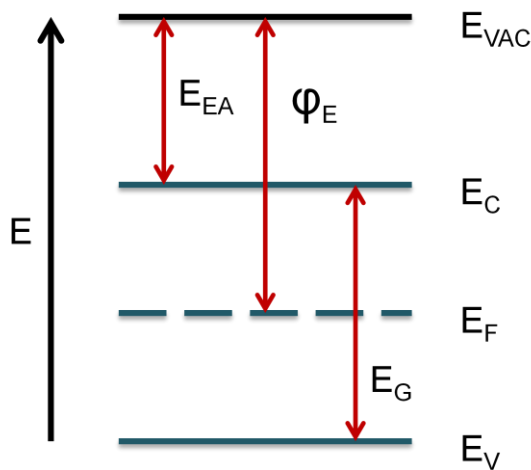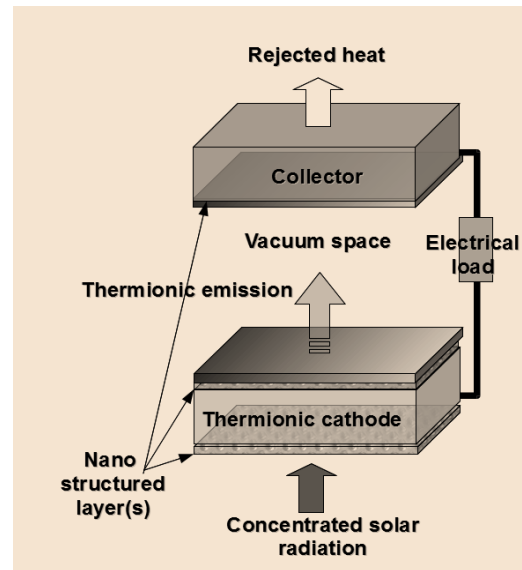

Figure 4

Figure 5

This paper examines how light trapping methods play an important role in optimising the absorption of incident radiation for an alternative method of generating electricity from solar power: thermionic converters. One major advantage that thermionic converters have over photovoltaic cells are that the absorbed wavelengths are not restricted by the semiconductor band gap[9], they are able to utilise a wider range of wavelengths to generate electricity. Thermionic converters work on the principle of thermionic emission, the heat induced flow of electrons from a surface due to thermal excitation of the material. The energy provided to the electrons has to exceed the material's work function; the minimum energy required to remove an electron from the solid to a

point outside the solid's surface. This is represented on Figure 4 as ϕ_E, the energy between the Fermi energy E_f and the vacuum energy E_{VAC}. Diamond is a material of particular interest for this application as it has a relatively low temperature at which electrons are ejected and can be produced with a negative electron affinity[10], meaning electrons can be emitted from its surface with little loss of energy. Figure 5[11] shows the basic structure of a thermionic converter. Solar radiation is absorbed by the thermionic cathode which then emits electrons to the collector, completing a circuit and allowing useful work to be done. The emitter must be able to absorb the incoming light, especially at wavelengths where the solar spectrum seen in figure 3 peaks.

The current density of thermionic emission, J, can be expressed by the Richardson-Dushman equation[12] (1)

$$J = AT^2 e^{-\frac{\varphi}{kT}} \qquad (1)$$

where A is a constant which includes factors pertaining to the band structure of the material and the back scattering of emitted electron back into the emitter. Equation 1 shows the current density is dependent on two key factors, the emitter work function ϕ and the emitter temperature. Light trapping plays an important role in attempting to maximise the temperature increase of the emitter to amplify the current extracted from the thermionic converter.

Another method used to achieve increased absorption of incident light is harnessing metallic nanostructures that support surface plasmons to direct light into the material to enhance absorption. It was initially of particular interest to thin film solar cells as it allows light trapping without the use of texturing[8]. Surface plasmons are collective oscillations of the conduction electrons in metal particles.
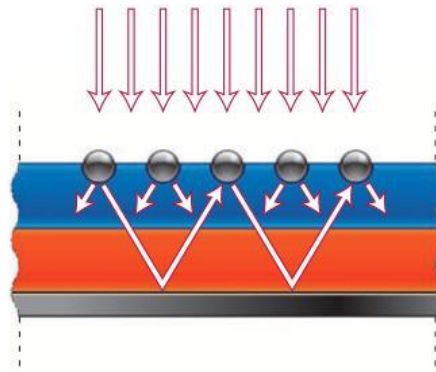

Figure 6

These electromagnetic oscillations can couple with incident light to form surface plasmon polaritons which can 'fold' the light into the semiconductor layer of a solar cell[3,8] or a thermionic emitter by increased scattering of escaping light back into the device, as shown in figure 6[3]. The light gains a spread of angles directed into the absorbing medium, increasing the optical path length. These plasmons can effectively be tuned to different resonances simply by changing the size and shape of the metal particles[8]. This allows for a large optical path length through the solar absorber for a wide range of wavelengths of light, maximising absorbing potential.
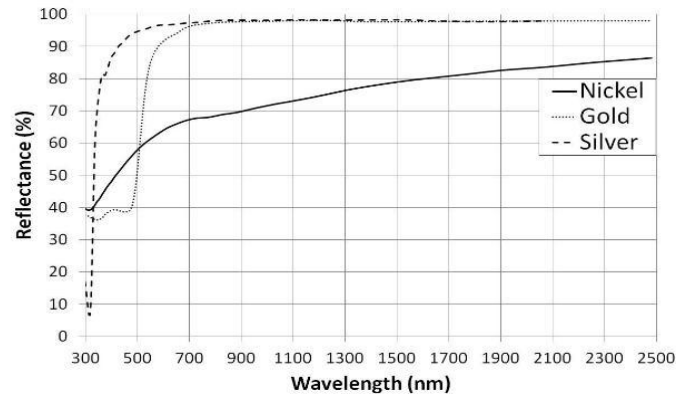
Figure 7

Ultra thin metal films have been examined as a way to increase absorption into thermionic materials. Figure 7[9] shows how a thin film of nickel demonstrates a naturally lower reflectivity across the visible and infra-red region. Another useful feature of nickel is that it has a melting point of 1453°C[9] which acts as a good compromise between surviving the operating temperatures of current thermionic devices and the ease of which nickel can be applied to thermionic surfaces. Two dimensional structuring of the nickel film, in the form of a 50 μm by 50 μm square grid, has achieved increased absorption of radiation into materials, conjectured to be due to a combination of micron scale diffraction and associated light trapping, and surface plasmon mediated temperature effects[13].

Future work in this field is looking interesting, with continued study into thin films and nanoparticles occurring with the intended incorporation of a beta radiation emitting layer into thermionic diamond converters. The aim of this is to improve the conversion of solar power into electrical energy and address the disposal of irradiated graphite from decommissioned Magnox and AGR nuclear reactors[13]. There has also been the recent introduction of 'Photon enhanced thermionic emission'[14] which looks towards increasing thermionic converter efficiency.

Experiment

Objective

Considering the importance of finding an efficient, low-cost alternative to conventional silicon solar cells as a means to generate electricity from the sun (and given the advantages of plasmonic and structural light trapping methods of increasing light absorption) this experiment examines the role of three dimensional structuring methods and plasmonic effects on the optical properties of a nickel etched diamond plasmonic absorber.

Method

Six specimens of a nickel etched diamond plasmonic absorber were produced using Microwave Chemical Vapour Deposition (MCVD), changing etch temperature and pressure to alter the fabrication process and produce different surface structures. Previously taken Focused Ion Beam (FIB) pictures were used alongside Scanning Electron Microscope (SEM) pictures to characterise the samples. The optical properties of the samples were measured using a visible/near infra-red spectrometer.

The diamond samples were produced in a two step process. Two 10 x 10 x 1 mm microcrystalline diamond (MCD) samples were prepared in the Bristol Diamond Lab by Dr Neil Fox. There were coated with a 10 nm thick nickel flat film, one sample coated on its rough side and the other on its smooth side. The samples were then cut into 5 x 5 x 1 mm pieces and then marked with a serial

number (1,2,3,4: smooth surface; 5,6,7,8: rough surface) using an Oxford Laser Systems (Oxford Inc., UK) laser cutter for the etching[15]. By using a hydrogen plasma treatment, nickel particles can be anisotropically etched into the diamond surface. Annealing of the Ni film at high temperature with a flow of H_2 over the surface causes the nickel layer to self assemble into nanoparticles to minimise the surface energy. The nanoparticles then catalytically etch the diamond[16]. A MCVD reactor using microwave radiation at 2.45 GHz produced by a 1.5 kW magnetron was used to produce a hydrogen plasma. The temperature was measured using a two wavelength optical pyrometer. Pairs of rough and smooth samples were put into the reactor on a molybdenum substrate holder under different conditions, except for samples 4 and 5, which were not treated with hydrogen plasma.

Table 1

Sample No. parameter	Group 1 No.1 and 6	Group 2 No.2 and 7	Group 3 No.3 and 8
Microwave power/kw	1.3	1.3	1.3
Temperature/°C	954	853	780
Time/mins	60	60	60
Hydrogen flow/SCCM	500	500	500
Pressure/Torr	200	150	100

Table 1[15] details the parameters of the etching process for each pair of samples.

Equipment
SEM images were taken with an Oxford 5600LV SEM (JEOL, Tokyo, Japan) and then visible spectroscopy measurements were carried out using a USB 2000+ Ocean Optics™ Spectrometer with bundled Spectrasuite™ software. This setup also used an Ocean Optics integrating sphere and an Ocean Optics HL-2000 light source. References were taken with a diffuse reflection standard.
Two sets of data were taken using the integrating sphere, and two using a fibre optic probe. The fibre optic probe has a central fibre surround by six others in a concentric circle. Either the central fibre or the six outer fibres can be used to illuminate the sample. All data was taken with an integration time of 1ms with each measurement being the average of 20 scans.

Unfortunately samples 4 and 5 were unavailable for characterization using FIB imaging and SEM imaging, whilst 1 and 4 were unavailable to undergo visible spectroscopy.
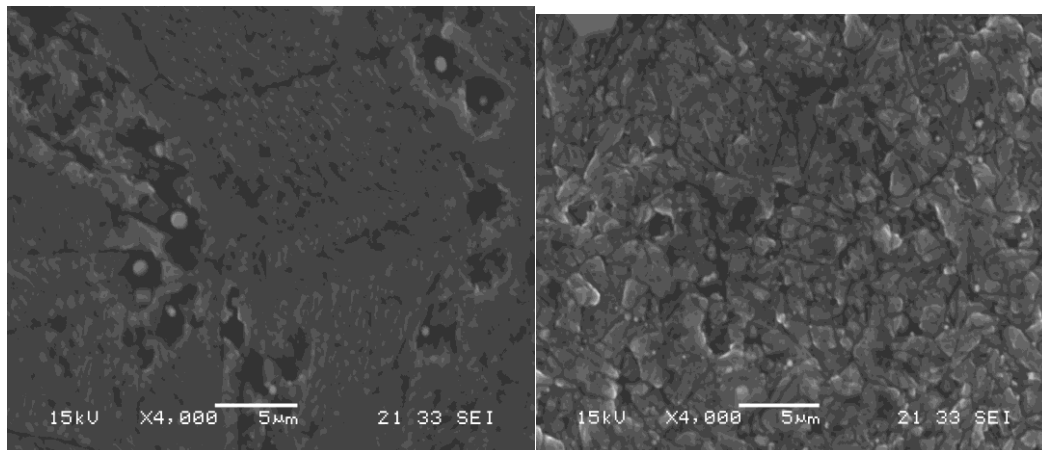
Data

SEM

Figure 8

Figure 8 shows SEM images of samples 2 (left) and 7 (right). 2 is the smooth side of the pair. It is possible to see the pits etched by the larger particles of nickel.
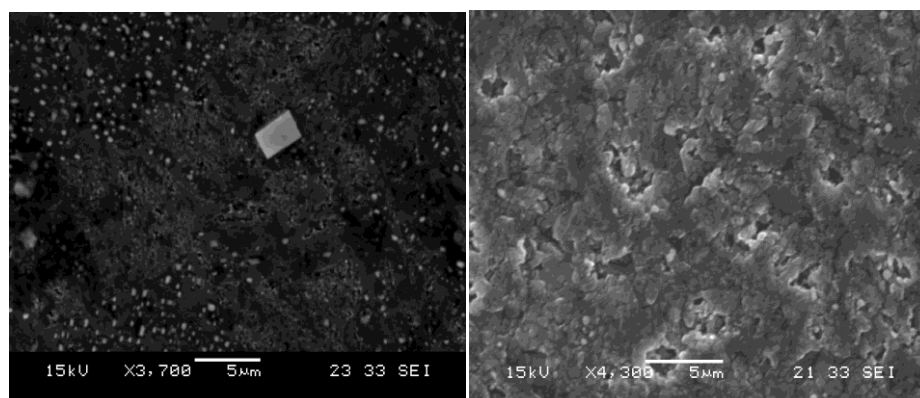

Figure 9

Figure 9 shows SEM images of samples 3 (left) and 8 (right). Etch pits are easily identifiable on sample 8 as they appear with a lighter shade rim around them.
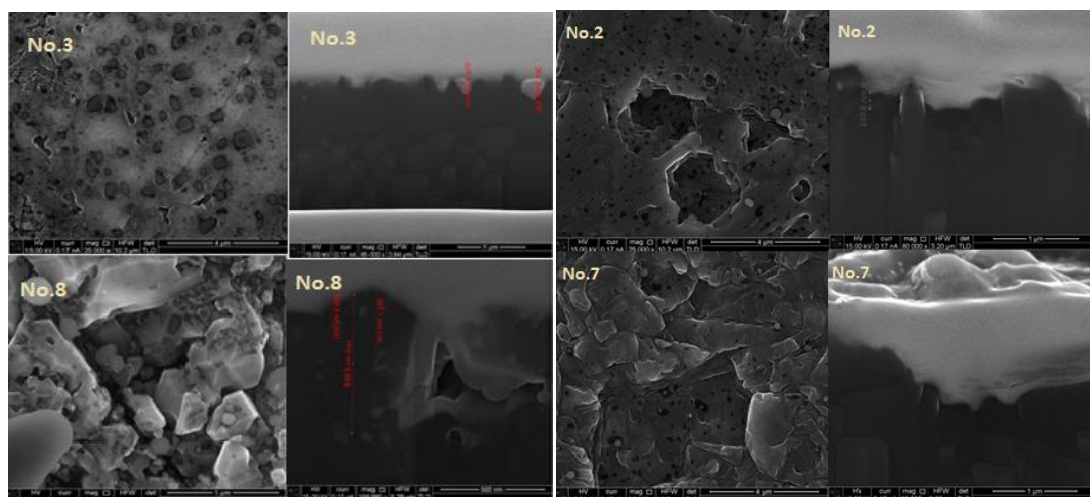
FIB[15]

Figure 10

Figure 10[15] shows the FIB plane and cross sectional images of samples 3, 8, 2 and 7. In samples 3 and 8 it can be seen that there are different sizes of nickel particles present in the surface of the samples, ranging from 20nm to 350nm, etched into the surface at depths between 200-850nm.
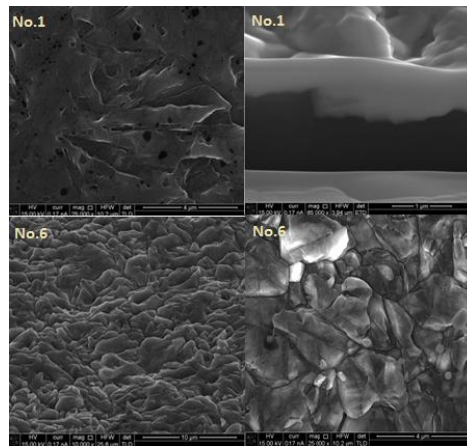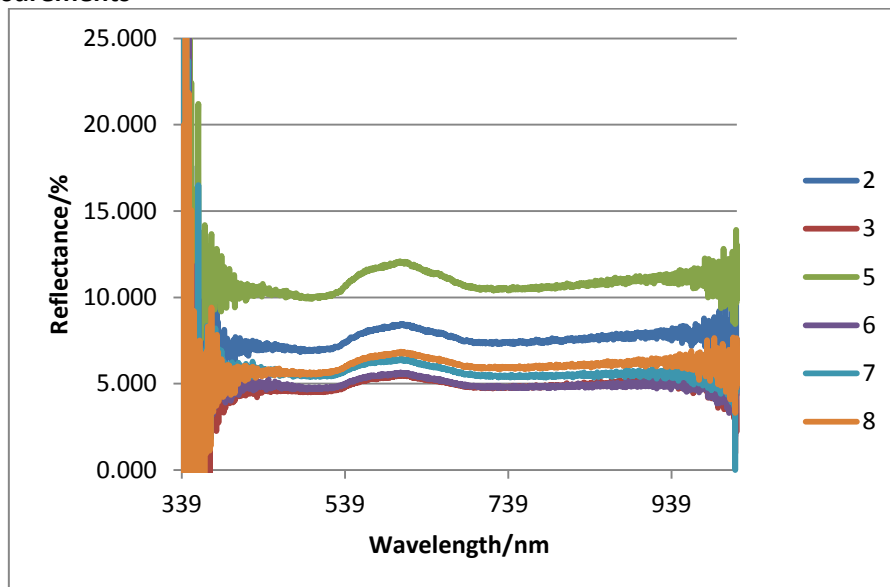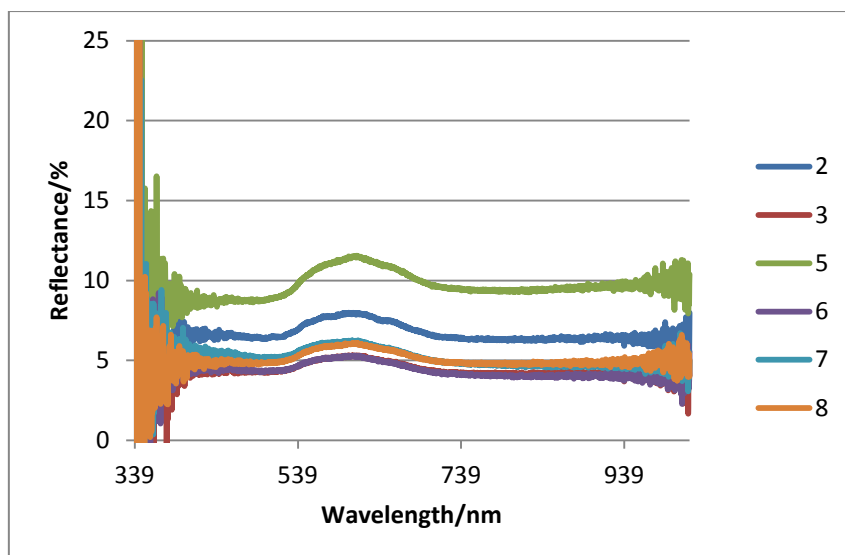

Figure 11

Figure 11[15] shows FIB plane and cross-sectional images of samples 1 and 6. There are almost no nickel particles present due to evaporation of the nickel during the etching process.
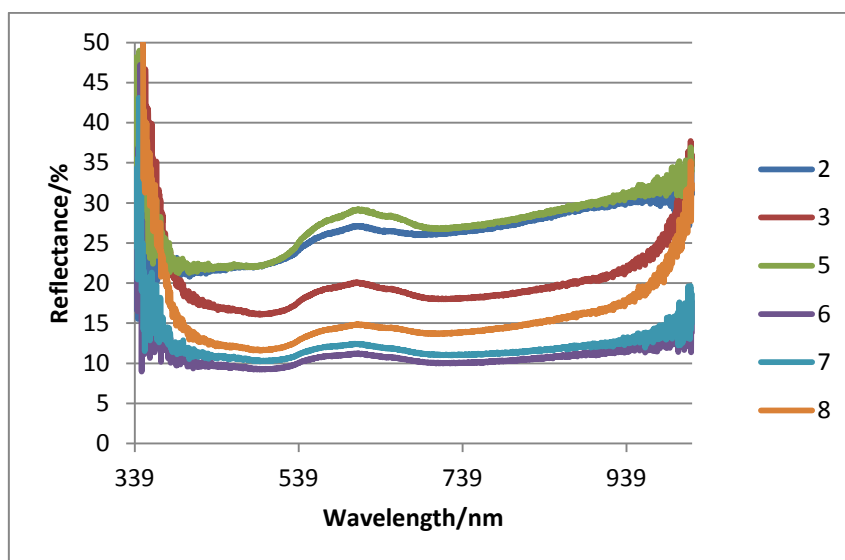
Optical Measurements

Graph 1

Graph 1 was taken using the integrating sphere. The data has the reflection spectra of the glass slide removed from each set of data. It shows sample 5, the rough diamond sample that was untreated by the hydrogen plasma, as the most reflective.
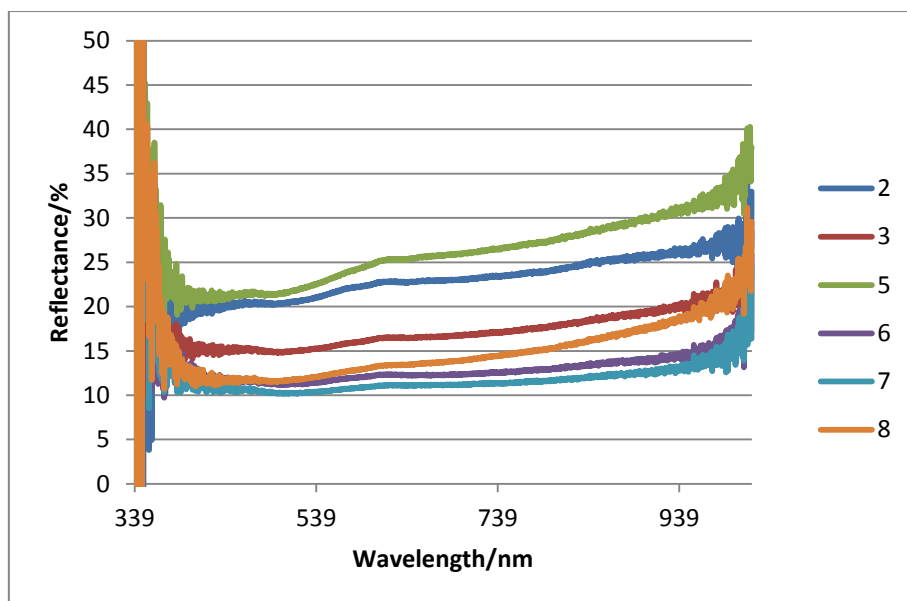
Graph 2

Graph 2 was taken using the integrating sphere. This graph has the reflection spectra of the glass slide removed from each set of data.
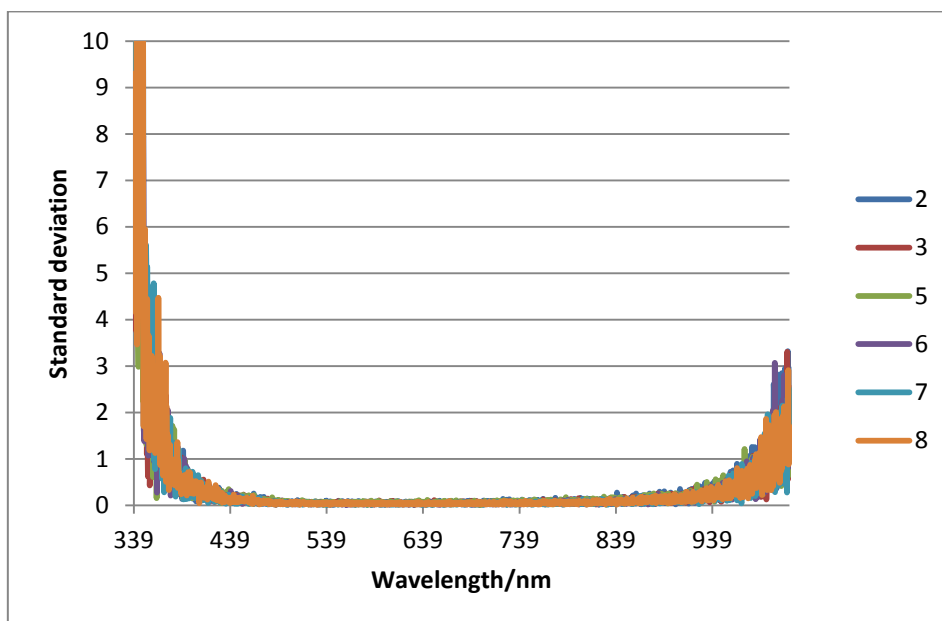

Graph 3

Graph 3 was taken using the fibre optic probe. The samples were illuminated using the 6 outer fibres and the reflection spectra were sampled using the central fibre.

Graph 4

Graph 4 was taken using the fibre optic probe. The samples were illuminated using the single, central fibre and the reflection spectra sampled using the six outer fibres.

Graph 5

Graph 5 shows the standard deviation of five spectra taken of the same sample, for each sample. This graph is typical of the error found with each spectroscopy equipment setup.

13

Discussion

Figure 12

Originally the absorbance measurements for the samples were to be calculated from reflectance and transmission, on the basis that the sum of the reflectance, transmittance and absorption would equal 100%. However, for transmission through the sample to register on the spectrometer the integration time on the spectroscopic software had to be set so high that when the sample was removed from in front of the light source the detector was overwhelmed by the intensity. It was decided that transmission was negligible for the purposes of this experiment and that absorption of the samples would be based off of reflectance only.

The initial integrating sphere setup proved to be inadequate due to the need to use a glass slide to hold the samples above the aperture in the apparatus, as shown in figure 12. This meant that light was reflected off the surface of the glass and channelled away from the sample, via total internal reflection, and out of the sides of the slide. This decreased the sensitivity of my results to changes in intensity. These results were deemed unreliable.
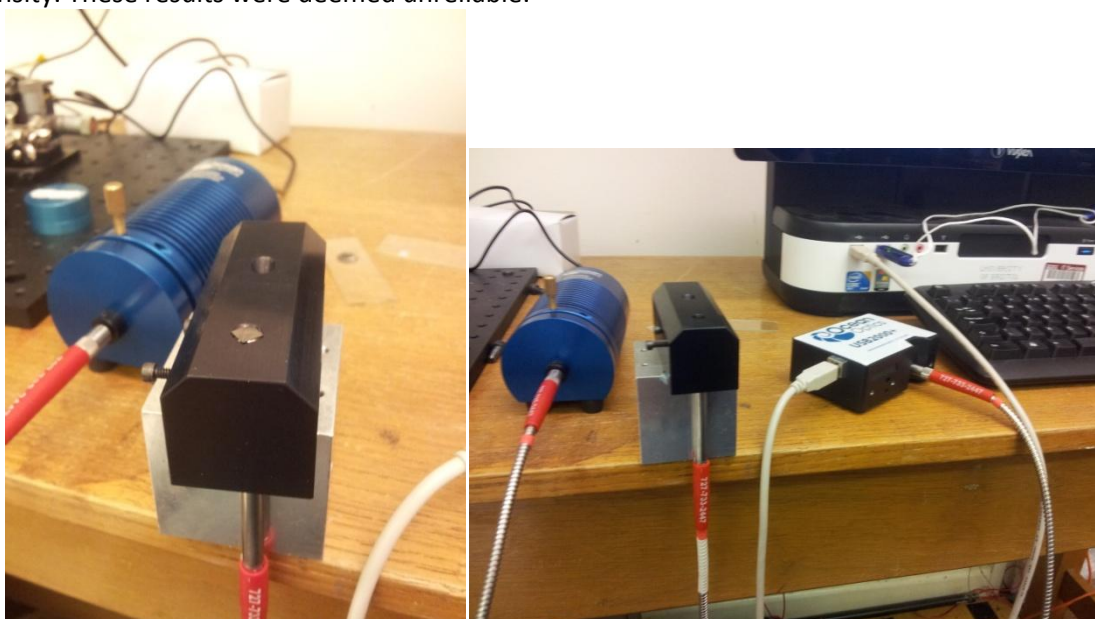

Figure 13

A new equipment setup was proposed, to eliminate use of the slide, where the fibre optic probe was clamped into a stand through a hole that was small enough to have the samples cover the top, as shown on the left in figure 13. Graphs 3 and 4 show less suppressed reflection data from all samples compared to graphs 2 and 3, and show good agreement between measurements. Following this data set some conclusions were drawn about the samples.

The next two most poorly absorbing samples were 2 and 3, both being smooth sided diamond. 2, the sample that had been treated at a higher temperature and pressure, absorbed a lot more poorly than 3. This indicates that on smooth sided diamond a slower, less aggressive etch creates a more favourable surface for absorption. This may be due to the increase evaporation of the nickel at the higher etch temperature and pressure, meaning there was less time to create significant surface structuring.

The next highest absorbing sample was sample 8, the rough sided diamond etched at the lowest pressure and temperature. The most absorbing samples were 6 and 7, altering places when the intensity of illumination changed between experiments. These were both rough sided diamond samples, etched at the higher temperatures and pressures where a lot of the nickel evaporated away. The high absorbance indicates that the etching possibly added increased texture to the rough surface and, if this was the case, it may be due to the rough surface aiding the formation of nickel spheres during etching. It is possible that the rough diamond samples naturally had better absorption than the smooth, even when the smooth were enhanced by the aid of the metal nanoparticles. Sample 5, the untreated nickel film on diamond was the worst absorber, despite it also being a rough surface, possibly due to the nickel layer forming a smooth surface.

The standard deviations in graph 5 show that the spectrometer suffers from a large amount of noise below ~440nm and above ~880nm, give only a small spectral window to provide reliable data.

Conclusions

It can be concluded from the data that for these samples surface roughness is bigger factor in absorption than plasmonic effects. On this topic smooth and rough diamond samples with no nickel applied at all should be measured alongside the diamond samples that have been etched, and that a larger range of temperatures and pressures for etching be investigated. Ideally the samples should be studied using apparatus that can simulate the solar spectrum seen at sea level. Further deliberation upon the use of the integrating sphere has led to the proposal that the device could be used inverted upon a sample, negating the need for a glass slide to stop a sample from falling inside.

References

1   BP (2012) *BP 2011 Statistical Review*. Available at: http://www.bp.com/statisticalreview (accessed 20th April 2013)

2   European Photovoltaic Industry Association (2013) *EPIA Press Release*. Available at: http://www.epia.org/news/press-releases/ (accessed 25th April 2013)

3   H. A. Atwater , A. Polman (2010) 'Plasmonics for improved photovoltaic devices' *Nature Materials* **9** pp.205-213

4   T. Markvart, L. Castaner (2003) *Practical handbook of photovoltaics: fundamentals and applications* Elsevier Advanced Technology: New York

5   M. A. Green, S. Pillai (2012)'Harnessing plasmonics for solar cells' *Nature Photonics* **6** pp.130-132

6   E. J. Yablonovitch (1982) 'Statistical ray optics' *Opt. Soc. Am.* **72**(7) pp.899-907

7   H. W. Deckman, C. B. Roxlo, E. J. Yablonovitch (1983) 'Maximum statistical increase of optical absorption in textured semiconductor films' *Opt. Lett.* **8** pp.491-493

8   S. Pillai, K. R. Catchpole, T. Trupke, M. A. Green (2007) 'Surface plasmon enhanced silicon solar cells' *J. Appl. Phys.* **101** 093105

9   N. ahmad, J. Stokes, N. A. Fox, M. Teng, M. J. Cryan (2012) 'Ultra-thin metal films for enhanced solar absorbtion' *Nano Energy* **1**(6) pp.777-782

10   I. L. Krainsky, V. M. Asnin (1998) 'Negative electron affinity mechanism for diamond surfaces' *Appl. Phys. Lett.* **72** 2574

11   E-ON (2008) Diamond nanoparticle energy converter for highly efficient solar generation Available at: http://www.eon.com/en/about-us/innovation/research-initiative/research-topic-2008/projects.html (Accessed 15th March 2013)

12   C. R. Crowell (1965) 'The Richardson constant for thermionic emission in Schottky barrier diodes' *Solid-State Electronics* **8** (4) pp.395–399

13   N.A. Fox , T.B. Scott, P.J. Heard, P.J. Flewitt, M.J. Cryan, N.L. Allan (2013) 'Energy and the Physical Sciences: Beta-enhanced thermionic energy converters and nuclear batteries employing nanostructured diamond electrodes' University of Bristol research proposal

14   J. W. Schwede et al. (2010) 'Photon-enhanced thermionic emission for solar concentrator systems' *Nature Materials* **9** 762–767

15   X. Zhang, N. Fox, M. Crane, P. Heard (2012) 'Surface plasmonic absorber for ultrathin solar energy' Bristol Centre for Functional Nanomaterials report

16   W. Smirnov et al. (2010) 'Anisotropic etching of diamond by molten Ni particles' *Appl. Phys. Lett.* **97** 073117